

Design of a Roller-Based Dexterous Hand for Object Grasping and Within-Hand Manipulation*

Shenli Yuan¹, Austin D. Epps², Jerome Nowak¹, J. Kenneth Salisbury³.

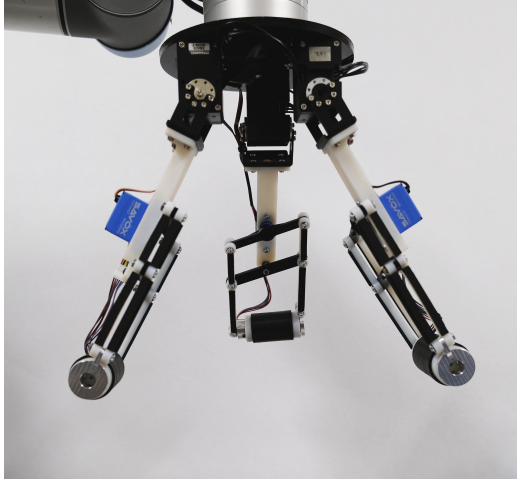


Fig. 1: The roller grasper prototype

Abstract—This paper describes the development of a non-anthropomorphic robot hand with the ability to manipulate objects by means of articulated, actively driven rollers located at the fingertips. Grasp and manipulation techniques for basic object shapes are explored analytically and validated experimentally. A system of equations for three-finger manipulation of a sphere is formulated and solved numerically to demonstrate full six degree of freedom non-holonomic spatial motion capability.

I. INTRODUCTION

In the pursuit of developing ever more capable robotic graspers, researchers have sought to match the remarkable dexterity of the human hand through mechanical means. A taxonomy for evaluating the dexterity requirements for an array of grasping tasks is presented in [1], in which the tasks requiring the most dexterity are both prehensile and within-hand. These are manipulations in which contact forces from the hand alone are used to grasp and stabilize the object, and where motion of the object is generated from the modulation of the contact forces between the hand elements and the grasped object. A robotic hand with the ability to perform within-hand manipulation possesses the ability to transition from the initial grasp configuration to other grasp configurations, for example to establish a more secure grasp

This research was supported, in part, by the Stanford Interdisciplinary Graduate Fellowship and Amazon Robotics

¹Department of Mechanical Engineering, Stanford University

²Dexterity Systems, LLC

³Department of Computer Science, Stanford University

shenliy@stanford.edu, austin@dexterity.systems,
jerome.nowak@stanford.edu, jks@cs.stanford.edu

by engaging object surfaces unavailable in the initial grasp orientation.

An extensive review of robotic hand designs in the past century is presented in [2]. Only a fraction of these hands have the capacity to perform within-hand manipulation tasks. The Stanford/JPL hand[3] and Utah/MIT hand[4] are among the earliest robotic hands possessing within-hand manipulation capabilities.

Because the human hand possesses the dexterity to perform within-hand manipulation, attempts have been made to replicate this ability by replicating its structure. Anthropomorphic hands, such as [5], [6], and [7] approximate the number of degrees of freedom (DoF) of the human hand and employ "traditional" fingers. The resulting robotic hands, while mechanically capable, have not found applications outside of the research lab due to their cost, sophisticated sensing and control requirements, and the sheer complexity of programming them to perform within-hand manipulation.

Another approach has been to focus on achieving grasping and manipulation capabilities with fewer actuated DoF such as [8], [9], and [10]. Many robotic hands also utilize under-actuated fingers in order for the hand to passively conform to the shape of the objects being grasped such as [11] and [12]. The use of under-actuated fingers provides increased grasp stability at the cost of reduced controllability, making within-hand manipulation more challenging. Within-hand manipulation using under-actuated fingers is an area of ongoing research, with recent examples provided by [13] and [14].

Highly non-anthropomorphic approaches to within-hand manipulation have also been explored. The incorporation of actuated conveyor belts was examined in [15] in order to enhance manipulation capabilities of a robotic grasper. This concept was further explored in recent works such as [16], [17], and [18]. Conveyor surfaces (or, more generically, "active surfaces") allow the graspers to impart motion to grasped objects without substantial modification of the grasp pose. In these embodiments the conveyor orientations are fixed, limiting object motion availability. In some sense our work generalizes these in that we explore imparting motion within a grasp by using active surfaces, in our case rotating cylinders, that can be placed against and oriented with respect to a grasped object.

II. DESIGN

A. Mechanical Design

The grasper assembly consists of three kinematically identical fingers (Fig. 2), each consisting of three actuated DoF. The proximal DoF is a revolute joint directly driven

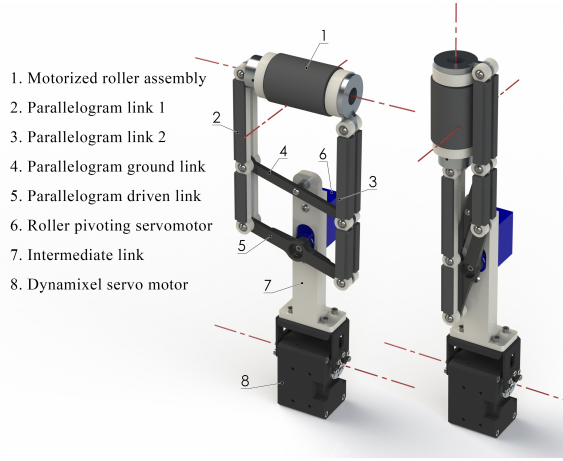


Fig. 2: Modular roller finger in the vertical configuration (left) and horizontal configuration (right). Locations of joint axes are shown in red.

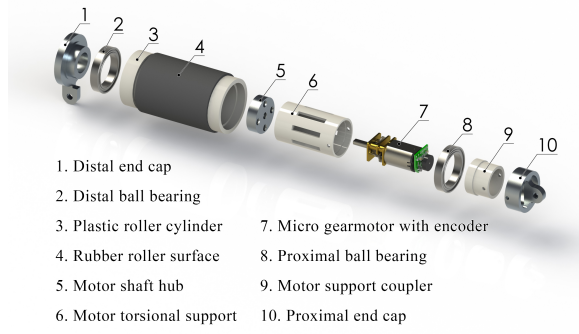


Fig. 3: Motorized roller assembly exploded view. Parts 3-5 and the outer race of 2 and 8 rotate with C_i , the others are fixed with B_i .

by a Robotis Dynamixel XM430-W350 smart actuator. The intermediate DoF is orthogonal to the proximal DoF, and is based on a parallelogram mechanism similar to [19] with the input and ground links anchored on the centerline of the parallelogram. The intermediate DoF controls the orientation of the fingertip roller, and is actuated by a micro digital servomotor (Savox SW0250MG). Neoprene strips are adhered to the faces of the two vertical links of the parallelogram mechanism so that they may be used as secondary grasping surfaces. The parallelogram configuration was selected in order to place the actuator further from the roller so as to maximize the area of the roller's surface that is available for grasping and within-hand manipulation. The fingertip roller (Fig. 3) is actuated by a micro DC gearmotor equipped with a quadrature encoder, and is capable of continuous rotation. The roller is fitted with a stack of square cross-section neoprene O-rings to provide a high-friction surface for grasping and manipulation.

The kinematic configuration and parameterization of the grasper assembly are shown in Fig. 4. Fingers 1 and 2 are arranged symmetrically and have parallel proximal joint

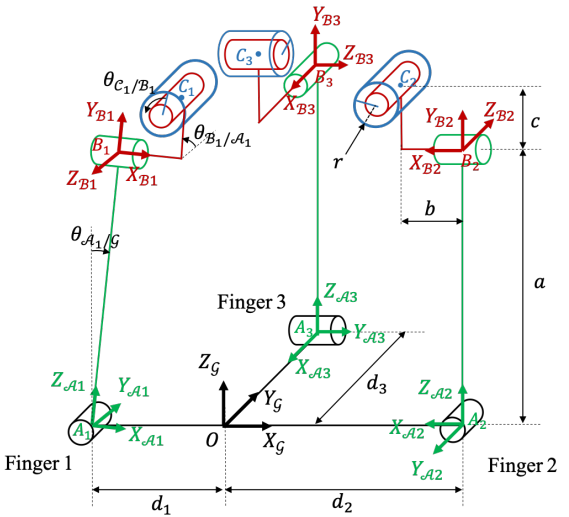


Fig. 4: 3D Kinematics. Joint angles for fingers 2 and 3 are defined similarly to finger 1, relative to local finger frames. Frame of reference \mathcal{G} is fixed to the wrist, and \mathcal{A}_i , \mathcal{B}_i , \mathcal{C}_i are the frames of the links in finger i . Here $\theta_{\mathcal{B}_1/\mathcal{A}_1} = \theta_{\mathcal{B}_3/\mathcal{A}_3} = -\theta_{\mathcal{B}_2/\mathcal{A}_2} = 90^\circ$.

axes. The parallelogram mechanisms of these two fingers are assembled in mirrored fashion such that when the roller is oriented vertically the vertical links connected to the tops of each roller assembly (Parallelogram link 2 in Fig. 2) are located on the same side of the grasper. Finger 3 is placed such that its proximal joint axis is orthogonal to the proximal joint axes of fingers 1 and 2, and this axis is offset from the shared midplane of fingers 1 and 2. It is placed such that when finger 3's roller is in the vertical configuration, the axis of the roller lies on the symmetry plane of fingers 1 and 2. Finger 3 has a parallelogram mechanism configuration identical to finger 1. Roller pivoting is constrained such that $\theta_{\mathcal{B}_1/\mathcal{A}_1} \in [0^\circ, 90^\circ]$, $\theta_{\mathcal{B}_2/\mathcal{A}_2} \in [-90^\circ, 0^\circ]$ and $\theta_{\mathcal{B}_3/\mathcal{A}_3} \in [0^\circ, 90^\circ]$. The configuration described here allows for several grasp and within-hand manipulation modalities which will be discussed in the following sections.

III. ANALYSIS

The hand's multiple degrees of freedom and contact surfaces result in a wide range of manipulation and grasping capabilities. To better understand the extent thereof, we present a kinematic analysis in the simplified case of 6-DoF spatial manipulation of a spherical object in contact with the rollers, with considerations on how further parametrization and computation could extend our analysis to other object classes (e.g. the ones manipulated experimentally). See Table I and Fig. 4 for notations and parameters used in this section. In this section frame \mathcal{G} is fixed with Z_G pointing vertically up.

A. Sphere Manipulation Configurations

Controlling motion relies on controlling the velocity vector applied at each contact point between the finger and the

TABLE I: Notation

Symbol(s)	Meaning
A	Point A.
\mathbf{A}	Vector giving the coordinates of A.
$\mathbf{X}_\mathcal{A}$	Unit vector defining the X axis of frame \mathcal{A} . If no frame is specified, frame \mathcal{G} is used.
${}^\mathcal{A}\mathbf{U}$	Vector \mathbf{U} expressed in frame \mathcal{A} . If no frame is specified, frame \mathcal{G} is used.
$R_{\mathbf{X}}, T_{\mathbf{X}}$	Classes of translations and rotations, respectively, around vector \mathbf{X}
$R_{\mathbf{X}_\mathcal{A}}(\theta)$	Rotation matrix around vector $\mathbf{X}_\mathcal{A}$ of a positive angle θ using the right hand rule, expressed in frame \mathcal{A} .
$\Omega_{\mathcal{B}/\mathcal{A}}$	Rotation velocity vector of frame \mathcal{B} relative to frame \mathcal{A} .

object, thus proper motion requires carefully steering the rollers. For simplicity, constraining each roller i to a vertical ($-\theta_{\mathcal{B}_i/\mathcal{A}_i} = 0^\circ$, abbreviated V) or horizontal ($\theta_{\mathcal{B}_i/\mathcal{A}_i} = 90^\circ$, abbreviated H) position, results in eight possible three-finger sphere manipulation configurations, and twelve possible two-finger ones. Considering the symmetrical combinations to be the same, this leaves six distinct three-finger and seven two-finger combinations.

Of the thirteen combinations, five were deemed particularly useful. The associated DoFs of the sphere when actuating the joints at A_i and B_i are presented Table II, assuming no slip. A manipulation configuration is described e.g. by HHV when rollers 1 and 2 are horizontal and roller 3 is vertical, and $HV\times$ when roller 1 is horizontal, 2 is vertical and 3 is unused. In addition, there exists a useful two-finger manipulation where fingers 1 and 2 transition in sync between H and V , as it provides pure x -rotation and is suitable for switching manipulation configuration, e.g. as an intermediate step from VVV to $HH\times$. Illustrations of these configurations are provided Fig. 7.

Table II demonstrates that sequentially combining those six manipulation configurations enables full 6-DoF spatial motion of a sphere. As some DoFs are coupled, certain pure motions are not instantaneously achievable due to the nonholonomic nature of the grasper. Such motions may be replicated using a succession of coupled motions, much like a car indirectly achieves a lateral translation by moving in forward and reverse while adjusting steering inputs during parallel parking. Other examples include uses of nonholonomic dexterous hands such as [20] and [21].

One should note that $VV\times$ is potentially unstable, as the sphere could roll out due to gravity e.g. during T_Y , though this is less of a concern for flat-faced objects, or for small objects and large forces thanks to roller surface compliance. A support contact with finger 3 can also aid in stabilizing the grasp.

Other manipulation configurations not considered here yield more complex, redundant or unstable motions, e.g. $HV\times$ (unstable) or HVV (couples T_Y with R_Z). Cases where $\theta_{\mathcal{B}_i/\mathcal{A}_i}$ have intermediate values are also possible but beyond the scope of this paper. Furthermore, these motions can analogously be applied to other convex objects as demonstrated in section IV with a six-sided die, though

TABLE II: Sphere manipulation - Degrees of freedom vs roller pivot angle

Roller Positions			Translation			Rotation		
1	2	3	T_X	T_Y	T_Z	R_X	R_Y	R_Z
H	H	\times	✓		✓		✓	
V	V	\times	✓ _{R_Y}	✓			✓ _{T_X}	✓
P	P	\times				✓		
V	V	H		✓	✓ _{R_X}	✓ _{T_Z}		
V	V	V		✓				✓
H	H	H			✓			

Notes: (1) all directions are relative to frame \mathcal{G} . (2) V means $\theta_{\mathcal{B}_i/\mathcal{A}_i} = 0^\circ$; H means $|\theta_{\mathcal{B}_i/\mathcal{A}_i}| = 90^\circ$; P means pivoting between H and V ; and \times means the finger is not used. (3) subscripts of ✓ indicate coupled motion and specify its nature.

TABLE III: Reference Frame Transformations

From frame	To frame	Homogeneous transformation matrix
\mathcal{G}	\mathcal{A}_1	${}^{\mathcal{G}}_1 T = \begin{bmatrix} R_{Y_\mathcal{G}}(\theta_{\mathcal{A}_1/\mathcal{G}}) & -d_1 {}^{\mathcal{G}}\mathbf{X}_\mathcal{G} \\ 0 & 0 & 0 & 1 \end{bmatrix}$
\mathcal{G}	\mathcal{A}_2	${}^{\mathcal{G}}_2 T = \begin{bmatrix} R_{Z_\mathcal{G}}(\pi)R_{Y_\mathcal{G}}(\theta_{\mathcal{A}_2/\mathcal{G}}) & d_2 {}^{\mathcal{G}}\mathbf{X}_\mathcal{G} \\ 0 & 0 & 0 & 1 \end{bmatrix}$
\mathcal{G}	\mathcal{A}_3	${}^{\mathcal{G}}_3 T = \begin{bmatrix} R_{Z_\mathcal{G}}(-\pi/2)R_{Y_\mathcal{G}}(\theta_{\mathcal{A}_3/\mathcal{G}}) & d_3 {}^{\mathcal{G}}\mathbf{Y}_\mathcal{G} \\ 0 & 0 & 0 & 1 \end{bmatrix}$
\mathcal{A}_i	\mathcal{B}_i	${}^{\mathcal{A}_i}_{\mathcal{B}_i} T = \begin{bmatrix} R_{\mathbf{X}_{\mathcal{A}_i}}(\theta_{\mathcal{B}_i/\mathcal{A}_i}) & a^{\mathcal{A}_i} \mathbf{Z}_{\mathcal{A}_i} \\ 0 & 0 & 0 & 1 \end{bmatrix}$
\mathcal{B}_i	\mathcal{C}_i	${}^{\mathcal{B}_i}_{\mathcal{C}_i} T = \begin{bmatrix} R_{Z_{\mathcal{B}_i}}(\theta_{\mathcal{C}_i/\mathcal{B}_i}) & b^{\mathcal{B}_i} \mathbf{X}_{\mathcal{B}_i} + c^{\mathcal{B}_i} \mathbf{Y}_{\mathcal{B}_i} \\ 0 & 0 & 0 & 1 \end{bmatrix}$

depending on their geometry slip might occur or motion availability may be restricted.

As a demonstration of how one would control a sphere, we present an in-depth analysis of three-finger VVH manipulation and two-finger $HH\times$ manipulation.

B. Example Three-Finger Manipulation

Using the homogeneous transformation matrices specified in Table III, a point designated by a vector ${}^{\mathcal{C}_i}\mathbf{U}$ in frame \mathcal{C}_i can be expressed in frame \mathcal{G} : ${}^{\mathcal{G}}\mathbf{U} = {}^{\mathcal{G}}_1 T {}^{\mathcal{A}_i}_{\mathcal{B}_i} T {}^{\mathcal{B}_i}_{\mathcal{C}_i} T [{}^{\mathcal{C}_i}\mathbf{U}]$.

Let \mathcal{D} be a spherical object of radius R and center \mathbf{D} contained within the workspace. Assuming the rollers are of infinite length, contact between \mathcal{D} and roller \mathcal{C}_i is expressed as:

$$\|\mathbf{Z}_{\mathcal{B}_i} \times (\mathbf{C}_i - \mathbf{D})\| = r + R \quad (1)$$

where

$$\begin{bmatrix} \mathbf{C}_i \\ 1 \end{bmatrix} = {}^{\mathcal{G}}_1 T {}^{\mathcal{A}_i}_{\mathcal{B}_i} T {}^{\mathcal{B}_i}_{\mathcal{C}_i} T [0 \ 0 \ 0 \ 1]^T \quad (2)$$

Furthermore, assuming there is no slip, the angles of roller \mathcal{C}_i and object \mathcal{D} can be computed using the no-slip condition at their point of contact:

$$\frac{d}{dt} \mathbf{I}_{\mathcal{D} \in \mathcal{C}_i} - \frac{d}{dt} \mathbf{I}_{\mathcal{C}_i \in \mathcal{D}} = \mathbf{0} \quad (3)$$

where $\mathbf{I}_{\mathcal{D} \in \mathcal{C}_i}$ is the point of \mathcal{C}_i that is momentarily coincident with \mathcal{D} , and $\mathbf{I}_{\mathcal{C}_i \in \mathcal{D}}$ is the point of \mathcal{D} that is momentarily

coincident with \mathcal{C}_i , and we choose to compute the derivatives in the center-of-momentum frame of \mathcal{D} (where we assume \mathcal{G} is inertial).

When $\theta_{\mathcal{A}_i/\mathcal{G}}$ and $\theta_{\mathcal{B}_i/\mathcal{A}_i}$ are known, we get a 2D solution space of possible ball positions for each finger, and in non-degenerate cases the intersection of all three-finger solutions gives a unique ball position for that configuration. When \mathcal{D} is known, (1) gives a 1D inverse kinematic solution space for $\theta_{\mathcal{A}_i/\mathcal{G}}$ and $\theta_{\mathcal{B}_i/\mathcal{A}_i}$, which can be reduced to one or two discrete joint positions by e.g. imposing $\theta_{\mathcal{B}_i/\mathcal{A}_i}$. We further discuss the existence of multiple solutions in the case of two-finger manipulation below. Solving (1) and (3) for all fingers allows us to numerically determine joint positions for within hand translation and rotation of a ball, and determine which movements will result in slip so as to avoid them. Generalizing to manipulating an arbitrary convex shape leaves (3) unchanged, and requires a 3D parametric equation of said shape to adapt (1) as well as considering object orientation.

A 3D kinematic simulation showing the manipulation configuration VVH was performed in MATLAB in the case of a sphere. A sequence from this simulation is shown in Fig. 5. If the no-slip condition is maintained at the contact surface of fingers 1 and 2, the only translation modality available for T_Z movement is rolling. To restrict rolling motion to be around \mathbf{X} , the contact points of fingers 1 and 2 are always symmetrical about the $\mathbf{Y}\text{-}\mathbf{Z}$ plane. Therefore, a translation T_Z induces a rotation R_X . The magnitude of R_X is inversely proportional to the effective rolling motion radius, i.e. the distance between the contact point with finger 1 or 2, and the axis going through D and carried by \mathbf{X} . Thus a smaller effective radius results in more rotation R_X per unit translation T_Z .

In the simulated sequence shown in Fig. 5, the rollers of fingers 1 and 2 translate the sphere from its initial pose (Fig. 5a) a distance of $+\Delta y$ along \mathbf{Y} while finger 3 provides stabilization of the sphere (Fig. 5b). The roller of finger 3 is then used to roll the sphere up along the surfaces of fingers 1 and 2 a distance of $+\Delta z$ and an angle $\Delta\theta_{x,1}$ (Fig. 5c). The effective radius R_1 of this rolling motion is displayed on the figure as an orange circle. The rollers of fingers 1 and 2 are once again used to translate the sphere a distance of $-\Delta y$ along \mathbf{Y} (Fig. 5d). Finally, the roller of finger 3 is used to roll the sphere a distance of $-\Delta z$ along \mathbf{Z} , with effective radius $R_2 < R_1$ and angle rotate $-\Delta\theta_{x,2}$ (Fig. 5e). The sphere's center has now returned to its original position, but has turned an angle of $\Delta\theta_x = \Delta z(1/R_1 - 1/R_2) < 0$. This allows the effective radius for T_Z movement to be changed independent of T_Y for successive up/down motions, thereby creating a non-holonomic circuit where the sphere may be translated from its initial pose through the circuit, arriving back at the initial cartesian position but with a net change in rotation R_X .

C. Example Two-Finger Manipulation

In the $HH\times$ configuration, 3-DoF manipulation of a convex object in the $\mathbf{X}\text{-}\mathbf{Z}$ plane is possible using the joints

at A_1 , A_2 , C_1 and C_2 . This can be described using (1) and (3), though the case of a spherical or cylindrical object \mathcal{D} can be regarded as a 5-bar geared linkage, whose forward and inverse kinematics have been explicitly solved in [22] (see Fig. 6). In the interest of implementing these explicit kinematics in our controller, we adapt the results in [22] to our vector-based notations and to the added symmetry of our design. For known joint angles $\theta_{\mathcal{A}_1/\mathcal{G}}$ and $\theta_{\mathcal{A}_2/\mathcal{G}}$ we have the forward kinematics equation:

$$\mathbf{D} = \frac{1}{2}(\mathbf{C}_1 + \mathbf{C}_2) \pm (\mathbf{C}_2 - \mathbf{C}_1) \times \mathbf{Y}_{\mathcal{G}} \sqrt{\frac{(r+R)^2}{\|\mathbf{C}_2 - \mathbf{C}_1\|^2} - \frac{1}{4}} \quad (4)$$

A positive sign in Eq. 4 has the ball resting on top of the rollers, while a negative sign has it below, held only by friction.

For a given ball position \mathbf{D} , there are two possible joint angles at A_1 and A_2 , given by the law of cosines:

$$\theta_{\mathcal{A}_i/\mathcal{G}} = \frac{\pi}{2} \pm \alpha_i(\mathbf{D}) - \beta_i(\mathbf{D}) - \gamma \quad (5)$$

where, with i in $\{1, 2\}$,

$$\alpha_i(\mathbf{D}) = \arccos\left(\frac{\|\mathbf{C}_i - \mathbf{A}_i\|^2 - (r+R)^2 + \|\mathbf{D} - \mathbf{A}_i\|^2}{2\|\mathbf{C}_i - \mathbf{A}_i\|\|\mathbf{D} - \mathbf{A}_i\|}\right) \quad (6)$$

$$\beta_i(\mathbf{D}) = |\operatorname{atan2}((\mathbf{D} - \mathbf{A}_i) \cdot \mathbf{Z}_{\mathcal{G}}, (\mathbf{D} - \mathbf{A}_i) \cdot \mathbf{X}_{\mathcal{G}})| \quad (7)$$

$$\gamma = \operatorname{atan2}(b, a+c) \quad (8)$$

$$\|\mathbf{C}_i - \mathbf{A}_i\| = \sqrt{(a+c)^2 + b^2} \quad (9)$$

Only one set of finger positions provides the most secure grasp with continuous manipulation capabilities. The following constraints narrow down the solutions to a negative sign in (5) for both fingers, and reduce the workspace \mathcal{G} can be in:

- viewed from above, the center of gravity of the sphere should be between rollers 1 and 2;
- the fingers should be applying forces toward each other in order to maintain a secure grasp.

With the above forward and inverse kinematic relationships between the positions of the fingers and that of the center of the ball, to take into account the rotations of \mathcal{D} , C_1 and C_2 , we need only write the no-slip condition (3) in this simplified case:

$$R\dot{\theta}_{\mathcal{D}/\mathcal{G}} = r(\dot{\theta}_{\mathcal{C}_1/\mathcal{B}_1} - \dot{\theta}_{\mathcal{A}_1/\mathcal{G}}) + (r+R)\dot{\theta}_{DC_1} \quad (10)$$

$$R\dot{\theta}_{\mathcal{D}/\mathcal{G}} = r(-\dot{\theta}_{\mathcal{C}_2/\mathcal{B}_2} + \dot{\theta}_{\mathcal{A}_2/\mathcal{G}}) + (r+R)\dot{\theta}_{DC_2} \quad (11)$$

where θ_{DC_i} is the angle between the vectors $\mathbf{X}_{\mathcal{G}}$ and $\mathbf{C}_i - \mathbf{D}$, counted positively towards $\mathbf{Y}_{\mathcal{G}}$.

We now have explicitly formulated 3-DoF planar forward kinematics with (4), (10) and (11), and inverse kinematics with (5), (10) and (11), which allows full 3-DoF planar motion.

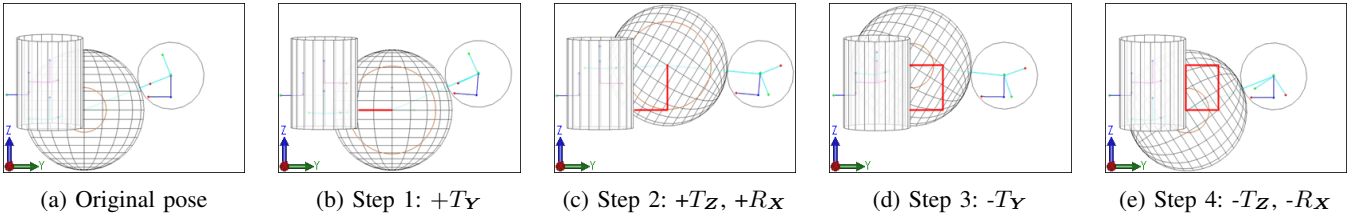


Fig. 5: Side view of 3D kinematic simulation demonstrating within-hand manipulation of a sphere. The path of the sphere center is shown by the red line segments. The effective radius of the rolling motion R_X , which only occurs during translation T_Z , is given by the orange circle, and is different between steps 2 and 4, resulting in a net rotation.

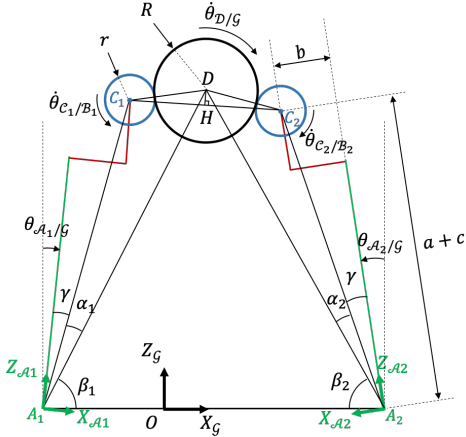


Fig. 6: 2D Kinematics

IV. EXPERIMENTS AND DISCUSSION

A proof-of-concept modular prototype (Fig. 1) was made to validate the analysis in section III and further explore manipulation and grasping capabilities. We mounted the grasper on two different bases: a tabletop one with Z_g pointing up, and a UR5 robotic arm.

A. Manipulation

All manipulation configurations referenced in Table II and Fig. 7 were experimentally validated with a range of sphere sizes, thus demonstrating fully controlled 6-DoF manipulation by transitioning between said configurations.

Furthermore, we successfully applied these capabilities to non-spherical objects of varying size, hardness and aspect ratio, such as a die (Fig. 9), a sheet of paper, the interior surface of a ring (Fig. 8a) or an open top box (Fig. 8b). The VVV configuration was also used to unscrew a bottle cap, with the threading pushing the cap up so it slipped vertically along the inside of the rollers. The fingers are pushed apart while maintaining contact via force control. Generally speaking, the hand can achieve controlled manipulation of objects with simple geometric features.

For fingertips without continuous rolling capabilities, motions like rotating a ball or turning a threaded object (e.g. a screw or bottle cap) are typically done by breaking and re-establishing contact, which can be complex to control or involve a supporting surface. In comparison, the grasper described here is particularly efficient for this. Manipulation

from inside an object is also a less common modality, which is enabled here by having most of the rollers' perimeter exposed, allowing the grasper to further extend its manipulation capabilities beyond its size limitations by fitting large objects around the outside of the fingers (e.g. in the case of the open top box).

B. Grasping

In addition to performing within-hand manipulation tasks, the presence of actively driven rolling fingertips offers benefits for grasping objects of different sizes, shapes, and properties. Several of the grasp techniques explored involve operating the rollers in a counter-rotating manner such that the grasped object is drawn into the grasper, allowing an object to be picked up without the assistance of external motion provided by a robot arm.

Figure 8 includes a list of grasp modalities we were able to perform successfully. These include:

- Picking up and manipulating a box via its inner faces using two fingers in the horizontal orientation (Fig. 8b). This modality allows for the grasping and manipulation of large boxes.
- Picking up a box via its exterior faces (Fig. 8c)
- Utilizing one roller in order to direct a thin object to the edge of a constraining surface where a second fingertip may establish a pinch grasp on the object (Fig. 8d).
- Grasping a flexible object, such as a piece of fabric, by taking advantage of its capacity for deformation. By operating the rollers in a counter-rotating manner while engaged with the flexible item, it is possible to draw the item into the rollers (Fig. 8e).
- Using the interior surfaces of the parallelogram mechanism vertical members of fingers 1 and 2 to provide motion on one side of an item, and the roller of finger 3 to provide motion on the opposite surface (Fig. 8f).
- Using the exterior surfaces of the parallelogram mechanism vertical members of fingers 1 and 2 and the roller of finger 3 to manipulate a box via its interior faces (Fig. 8g).
- Grasping and manipulating a box via its interior faces using all three fingers for a more stable grasp (Fig. 8h).

C. Limitations

1) *Non-holonomic nature*: The system is non-holonomic, as the grasped object cannot be moved in an arbitrary

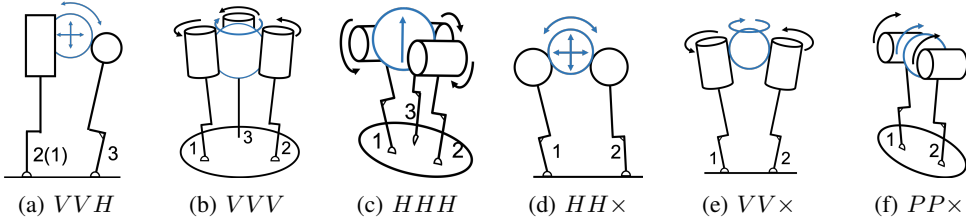


Fig. 7: Roller positions for the manipulation of a spherical object

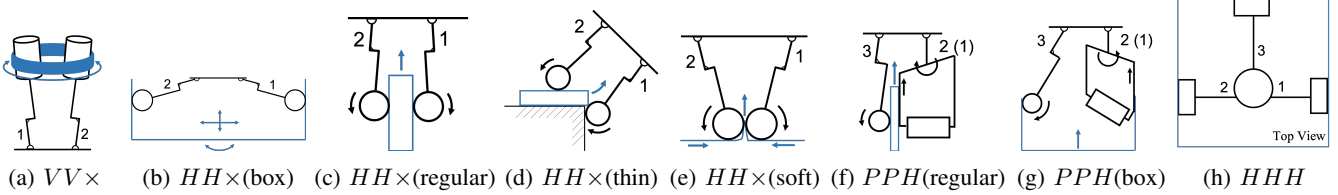


Fig. 8: Other roller positions (Fig. 8a for manipulation; 8b for manipulation and grasping; the rest for grasping)

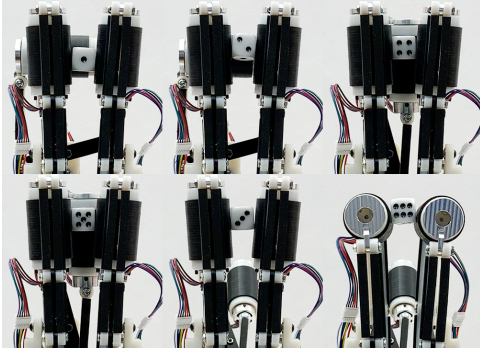


Fig. 9: Manipulation of a six-sided die to show all faces of a cube. Transitions are, in sequence from left to right, top to bottom: $VVH(R_X \& T_Z)$, $VVV(R_Z)$, $VVV(R_Z)$, $VVV(R_Z)$, $PP \times (R_X)$

direction instantaneously. The object may need to go through a series of link motions before reorientation can be achieved to a certain pose (e.g. rolling an object in the Z direction when the two rollers are horizontal).

2) *Slipping & Undefined manipulation:* When there is not enough contact area between the roller and the object, the object might slip, causing inaccuracy in the manipulation. Slipping can happen in different cases but most likely to in three-finger manipulation when all three rollers are vertical, the object only has point contacts with two or more rollers and the weight of object is relatively large compared to the friction generated by grasping.

3) *power grasping limitations:* Although each finger has three DoF, two of the DoF contribute to the motions of the rollers. As a result, for some objects being grasped, it would be difficult for the grasper to conform onto the shape of the object. Therefore the grasper can perform pinch grasp very well, especially with the help of rollers, but cannot perform power grasp except for a small subset of objects (thin and long objects can be constrained between the area connecting the link and the roller).

V. CONCLUSIONS & FUTURE WORK

This paper describes the preliminary design and control of a robot hand that can manipulate objects by using the rolling motion of powered cylindrical fingertips. The hand mechanism enables aligning each fingertip axis of rotation where it contacts an object to be manipulated. We have derived the kinematic equations for planar motion and demonstrated their use in full 3-DoF planar motion. In addition, we have demonstrated full 6-DoF spatial motion of a grasped object. In the current embodiment, it is actually not possible to specify the exact rolling axis direction and the precise object contact point simultaneously. This could be resolved by using a zero-length cylinder (a wheel). Even with this alteration, the system is still non-holonomic, in that it cannot move an object in an arbitrary direction instantaneously - the cylinders must be aligned correctly before we can proceed with arbitrary motion. This constraint could be removed by using spherical fingertips able to rotate in two independent directions. While analysis requiring the Jacobian (or more properly, the Grasp Matrix [3]) is required for controlling grasp forces and object differential motions, it is beyond the scope of this preliminary study. The hand we presented takes a decidedly non-anthropomorphic approach to within-hand manipulation. It raises interesting and important questions about control and planning, as well as mechanism design. Future work includes developing various control schemes for controlled slipping during 3 finger manipulation, dynamic analysis of the roller grasper and redesign of the finger and roller mechanism.

ACKNOWLEDGMENT

The authors would like to express their appreciation to Keven Wang and UnitX, Inc. for use of their robot and facilities during our experimental validations.

REFERENCES

- [1] I. M. Bullock and A. M. Dollar, "Classifying human manipulation behavior," in *2011 IEEE International Conference on Rehabilitation Robotics*, IEEE, 2011.

- [2] C. Piazza, G. Grioli, M. Catalano, and A. Bicchi, "A century of robotic hands," *Annual Review of Control, Robotics, and Autonomous Systems*, vol. 2, pp. 1–32, 2019.
- [3] J. Salisbury, "Kinematics and force analysis of articulated hands, phd thesis," 1982.
- [4] S. C. Jacobsen, J. E. Wood, D. Knutti, and K. B. Biggers, "The Utah/MIT dexterous hand: Work in progress," *The International Journal of Robotics Research*, vol. 3, no. 4, pp. 21–50, 1984.
- [5] M. Diftler *et al.*, "Robonaut 2- the first humanoid robot in space," in *Proceedings of the IEEE International Conference of Robotics and Automation*, pp. 2178 – 2183, IEEE, 2011.
- [6] "Design of a dexterous hand for advanced CLAWAR applications," tech. rep., Shadow Robot Company, 2003.
- [7] M. Grebenstein *et al.*, "The DLR hand arm system," in *2011 IEEE International Conference on Robotics and Automation*, pp. 3175–3182, May 2011.
- [8] R. Ma and A. Dollar, "Yale openhand project: Optimizing open-source hand designs for ease of fabrication and adoption," *IEEE Robotics & Automation Magazine*, vol. 24, no. 1, pp. 32–40, 2017.
- [9] R. R. Ma, L. U. Odhner, and A. M. Dollar, "A modular, open-source 3d printed underactuated hand," in *2013 IEEE International Conference on Robotics and Automation*, pp. 2737–2743, IEEE, 2013.
- [10] W. G. Bircher, A. M. Dollar, and N. Rojas, "A two-fingered robot gripper with large object reorientation range," in *2017 IEEE International Conference on Robotics and Automation (ICRA)*, pp. 3453–3460, IEEE, 2017.
- [11] A. M. Dollar and R. D. Howe, "The highly adaptive SDM hand: Design and performance evaluation," *The international journal of robotics research*, vol. 29, no. 5, pp. 585–597, 2010.
- [12] S. B. Backus and A. M. Dollar, "An adaptive three-fingered prismatic gripper with passive rotational joints," *IEEE Robotics and Automation Letters*, vol. 1, no. 2, pp. 668–675, 2016.
- [13] R. R. Ma and A. M. Dollar, "An underactuated hand for efficient finger-gaiting-based dexterous manipulation," in *2014 IEEE International Conference on Robotics and Biomimetics (ROBIO 2014)*, pp. 2214–2219, IEEE, 2014.
- [14] C. M. McCann and A. M. Dollar, "Design of a stewart platform-inspired dexterous hand for 6-DOF within-hand manipulation," in *2017 IEEE/RSJ International Conference on Intelligent Robots and Systems (IROS)*, pp. 1158–1163, IEEE, 2017.
- [15] P. Datseris and W. Palm, "Principles on the development of mechanical hands which can manipulate objects by means of active control," *Journal of Mechanisms, Transmissions, and Automation in Design*, vol. 107, no. 2, pp. 148–156, 1985.
- [16] N. Govindan and A. Thondiyath, "Design and analysis of a multimodal grasper having shape conformity and within-hand manipulation with adjustable contact forces," *Journal of Mechanisms and Robotics*, vol. 11, 2019.
- [17] V. Tincani, M. G. Catalano, E. Farnioli, M. Garabini, G. Grioli, G. Fantoni, and A. Bicchi, "Velvet fingers: A dexterous gripper with active surfaces," in *2012 IEEE/RSJ International Conference on Intelligent Robots and Systems*, pp. 1257–1263, IEEE, 2012.
- [18] R. R. Ma and A. M. Dollar, "In-hand manipulation primitives for a minimal, underactuated gripper with active surfaces," in *ASME 2016 International Design Engineering Technical Conferences and Computers and Information in Engineering Conference. American Society of Mechanical Engineers*, pp. V05AT07A072–V05AT07A072, 2016.
- [19] R. H. Taylor, J. Funda, D. D. Grossman, J. P. Karidis, and D. A. LaRose, "Remote center-of-motion robot for surgery," Mar. 14 1995. US Patent 5,397,323.
- [20] A. Bicchi and R. Sorrentino, "Dexterous manipulation through rolling," in *Proceedings of 1995 IEEE International Conference on Robotics and Automation*, vol. 1, pp. 452–457, IEEE, 1995.
- [21] A. Bicchi, A. Marigo, and D. Prattichizzo, "Dexterity through rolling: Manipulation of unknown objects," in *Proceedings 1999 IEEE International Conference on Robotics and Automation (Cat. No. 99CH36288C)*, vol. 2, pp. 1583–1588, IEEE, 1999.
- [22] G. Campion, "The pantograph MK-II: a haptic instrument," in *The Synthesis of Three Dimensional Haptic Textures: Geometry, Control, and Psychophysics*, pp. 45–58, Springer, 2005.